Journal of Biomechanics 44 (2011) 622–629

Contents lists available at ScienceDirect

Journal of Biomechanics

journal homepage: www.elsevier.com/locate/jbiomech
www.JBiomech.com

Characterization of blood clot viscoelasticity by dynamic ultrasound elastography and modeling of the rheological behavior

Cédric Schmitt [a,b], Anis Hadj Henni [a], Guy Cloutier [a,b,c,*]

[a] Laboratory of Biorheology and Medical Ultrasonics, Research Center, Centre hospitalier de l'Université de Montréal (CRCHUM), Montréal, Québec, Canada H2L 2W5
[b] Institute of Biomedical Engineering, Université de Montréal, Montréal, Québec, Canada H3C 3J7
[c] Department of Radiology, Radio-Oncology and Nuclear Medicine, Université de Montréal, Montréal, Québec, Canada H3T 1J4

ARTICLE INFO

Article history:
Accepted 10 November 2010

Keywords:
Dynamic elastography
Ultrasound imaging
Plane shear wave
Blood coagulation kinetics
Storage modulus
Loss modulus
Viscoelasticity
Mechanical properties
Rheological models

ABSTRACT

Dynamic elastography (DE) is a new tool to study mechanical behavior of soft tissues via their motion response to propagating shear waves. This technique characterized viscoelasticity of 9 porcine whole blood samples (3 animals) during coagulation for a shearing frequency of 70 Hz, and after complete clot formation between 50 and 160 Hz. Clot storage (G') and loss (G'') moduli were calculated from shear wave velocity and attenuation. Temporal evolutions of G' and G'' during coagulation were typified with 4 parameters: maximum change in elasticity (G' $slope_{max}$), elasticity after 120 min of coagulation (G'_{max}), time occurrence of G'' maximum (t_e) and G'' at the plateau ($G''_{plateau}$). G' and G'' frequency dependence of completely formed blood clots was fitted with 5 standard rheological models: Maxwell, Kelvin–Voigt, Jeffrey, Zener and third-order generalized Maxwell. DE had sufficient sensitivity to follow the coagulation kinetics described by a progressive increase in G', while G'' transitory increased followed by a rapid stabilization. Inter- and intra-animal dispersions (InterAD and IntraAD) of G'_{max} (InterAD=15.9%, IntraAD=9.1%) showed better reproducibility than G' $slope_{max}$ (InterAD=40.4%, IntraAD=21.9%), t_e (InterAD=27.4%, IntraAD=18.7%) and $G''_{plateau}$ (InterAD=58.6%, IntraAD=40.2%). G' evolution within the considered range of frequency exhibited an increase, followed by stabilization to a plateau, whereas G'' presented little variations with convergence at a quasi-constant value at highest frequencies. Residues χ^*, describing the goodness of fit between models and experimental data, showed statistically ($p<0.05$) that the Kelvin–Voigt model was less in agreement with experimental data than other models. The Zener model is recommended to predict G' and G'' dispersion of coagulated blood over the explored frequency range.

1. Introduction

Deep venous thrombosis (DVT) is a vascular disease characterized by the formation of blood clots or thrombi in lower limb veins that can lead to pulmonary embolism. Thrombus maturity, related to its age-dependent elasticity (Geier et al., 2005; Xie et al., 2005), is important for its classification (Zwiebel, 2004) and, thus, for identifying an appropriate therapy. Recently, dynamic elastography (DE) methods were proposed to characterize the viscoelasticity of biological tissues (Muthupillai et al., 1995; Sarvazyan et al., 1998). These novel non-invasive and quantitative approaches first imply generation of properly polarized, low-frequency, harmonic or transient shear waves in the medium, and tracking of these waves with ultrasound (Taylor et al., 2000; Sandrin et al., 2002; Catheline et al., 2004; Bercoff et al., 2004), magnetic resonance (Kruse et al., 2000; Sinkus et al., 2000) or laser-based approaches (Bossy et al., 2007; Bouchard et al., 2009). A major advantage of DE is that it can be adapted to image, in real time, mechanical displacements provoked by shear wave motion, thus potentially allowing an *in vivo* mechanical characterization of DVT. Most DE methods employ a reconstruction algorithm, which retrieve mechanical parameters of probed medium by assuming a certain viscoelastic behavior. The choice of the most adequate viscoelastic model is essential to improve mechanical estimates. It is thus obvious that developing DE for DVT application requires accurate knowledge of blood viscoelastic properties during clotting and after complete coagulation.

A wide variety of *in vitro* techniques has been proposed to characterize blood viscoelasticity during and after clotting. Among quantitative methods, rotational rheometers were used to measure storage (G') and loss moduli (G'') (Burghardt et al., 1995; Riha et al., 1999; Williams et al., 2006; Evans et al., 2008a). However, uncertainty of sample geometries due to handling restrictions can imply measurement errors, whereas difficulties in imposing perfect non-slipping contact between the blood clot and rotating plates limit these instruments to a range of frequencies typically below 10 Hz.

One-dimensional (1-D) ultrasound DE, introduced by Sandrin et al. (2002) and adapted by Gennisson et al. (2006a) to blood clot

* Corresponding author at: Laboratory of Biorheology and Medical Ultrasonics, CRCHUM, 2099 Alexandre de Sève, Room Y-1619, Montréal, Québec, Canada H2L 2W5. Tel.: +1 514 890 8000 (24703); fax: +1 514 412 7505.
E-mail address: guy.cloutier@umontreal.ca (G. Cloutier).

0021-9290/$ - see front matter © 2010 Elsevier Ltd. All rights reserved.
doi:10.1016/j.jbiomech.2010.11.015

mechanical characterization allowed to quantitatively detect changes in viscoelasticity during clotting and proved to be sensitive to variations in hematocrit, fibrinogen and heparin concentrations. However, the latter study, carried out at a single frequency (25 Hz) and assuming a Kelvin–Voigt viscoelastic model, gave biased viscosity values because of the 1-D formulation, chosen mechanical model, and shear wave generation strategy.

In this context, the present study is filling the lack of information about G' and G'' evolution during whole blood clotting and explores clot rheological behavior over a large frequency range (50–160 Hz) with DE. This range of frequency is justified by the abovementioned DVT application, for which image resolution improves with frequency but image quality degrades with frequency-dependent attenuation of shear waves. Velocities (v) and attenuations (α) of plane shear waves propagating into large and homogeneous blood clots as a function of time or frequency were estimated to calculate the complex shear modulus ($G=G'+iG''$). The frequency dependence of G was fitted to different rheological laws to find which model better reproduces the dynamic mechanical behavior of blood clots. The reproducibility and variability of measurements with different porcine blood samples were also investigated.

2. Methods

2.1. Experimental set-up

The experimental set-up was composed of a large rigid plate (202×85 mm^2) attached to a vibrator (Type 4810, Brüel & Kjær, Nærum, Denmark) and applied on the phantom surface (Fig. 1). A low-frequency 20-period harmonic excitation (50–160 Hz) was produced by a function generator (Model 33250 A, Agilent, Palo Alto, CA, USA) configured using the general purpose interface bus (GPIB) and amplified (Type 2706 low-frequency amplifier, Brüel & Kjær) before supplying the vibrator. A clinical ultrasound array transducer (L14-5/38, Ultrasonix) of a Sonix RP scanner (Ultrasonix Medical Corporation, Burnaby, BC, Canada) was positioned parallel to displacements of scatterers within the phantom to acquire and reconstruct radio-frequency (RF) sequences (see details below). The excitation frequency of the probe, sampling frequency and bit depth were 10 MHz, 40 MHz and 16 bits, respectively. An electronic circuit (SYNCH) was designed to properly synchronize the RF image acquisition with the shear wave pulsation for retrospective RF image reconstructions. Experiments were conducted in a temperature-controlled chamber at 20 °C.

Phantom-building consisted of pouring an agar (3% w/w)–gelatin (4% w/w) mixture (Gennisson and Cloutier, 2006b) into a $20.5 \times 27.5 \times 10.5$ cm^3 hollow box containing a $8 \times 10 \times 3.5$ cm^3 parallelepiped inclusion that was filled with fresh porcine blood. Coagulation was initiated by adding 2 g/L$_{blood}$ of calcium ions ($CaCl_2$, calcium chloride dihydrate, Acros Organics, Geel, Belgium) diluted into 40 mL/L$_{blood}$ of saline solution. The reproducibility and variability of blood clot viscoelastic properties were tested with 9 blood samples, withdrawn from 3 different healthy animals (3 samples per animal), and experiments were performed within 16 h of blood sampling.

2.2. Acquisition of RF sequences and post-processing

Immediately after adding $CaCl_2$ to blood, the mixture was poured into the inclusion footprint. This time defined the beginning of experiments consisting in acquiring RF sequences every 4 min for 2 h, and tracking the 70-Hz shear wave propagation into the inclusion. To study viscoelasticity, a multi-frequency strategy, which consisted of repeating the above procedure at frequencies from 50 to 160 Hz with a step of 10 Hz, was then undertaken on the previously described phantom after complete blood coagulation (3 h after the beginning of data acquisition).

To overcome the scanner frame rate limit (i.e., ~250 images/s for small regions of interest), high frame rate RF sequences were retrospectively reconstructed to follow shear wave propagation without aliasing. As outlined by Hadj Henni et al. (2008), the 128 transducer array elements were sequentially activated in 64 groups of two elements. At each firing of pairs of elements, the low-frequency shear wave vibration was synchronized and generated within the phantom. The scanner then acquired 1000 consecutive frames at a high frame rate of 3850 images/s. This process was repeated for each group of elements. Off-line, retrospective post-processing consisted of re-assembling measured RF echoes to reconstruct the matrix width × depth × time (38-mm × 80-mm × 260-ms) of each image frame. Successive ultrasonic signal propagation paths over time were processed with a 1-D cross-correlation algorithm to compute shear wave motion along the x-axis within the blood medium (see Fig. 1).

2.3. Theory

Let an infinite medium be homogeneous, isotropic, linear, viscoelastic and incompressible. The displacement field induced by the propagation of a harmonic plane shear wave is then described by the Navier differential equation (Achenbach, 1973). If one assumes a plane shear wave $U_y(x,t)$ propagating in the x direction and

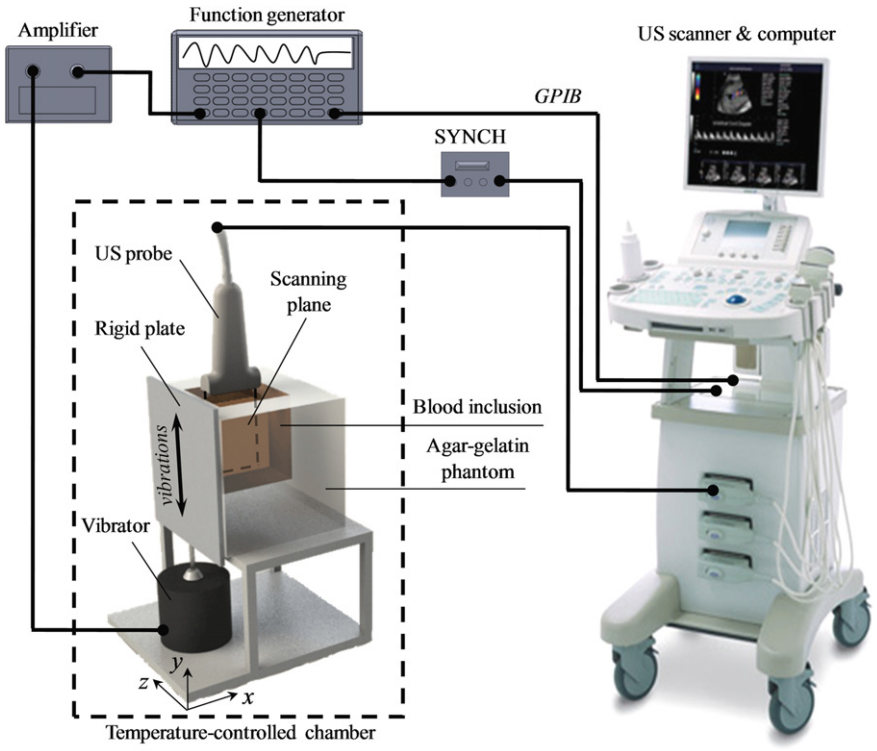

Fig. 1. *In vitro* experimental set-up used to generate and track shear waves for dynamic ultrasound elastography (DE).

polarized in the y direction (Fig. 1), the displacement differential equation is reduced to the Helmholtz wave equation

$$G(\omega)\frac{\partial^2 U_y(x)}{\partial x^2}+\rho\omega^2 U_y(x)=0 \quad (1)$$

where $G(\omega)$ is the complex shear modulus, $U_y(x)$ is the wave amplitude $U_y(x,t)=U_y(x)e^{i\omega t}$ and ρ is the material density assumed constant at 1080 kg/m^2 (Nahirnyak et al., 2006). Because harmonic plane shear waves were used, the time dependence can be omitted for simplification. The stationary shear wave amplitude $U_y(x)$ solving Eq. (1) has the following form:

$$U_y(x)=U_0 e^{i(k'+i\alpha)x}e^{i\phi} \quad (2)$$

where U_0 denotes the absolute wave amplitude and ϕ is an arbitrary phase (indeed, generated shear waves are pseudo-harmonic with only 20 periods). Parameters k' and α designate the real (velocity) and imaginary (attenuation) parts of the wave number, respectively. The wave velocity v was calculated from the wave number real part k', and wave angular frequency ω as

$$v=\frac{\omega}{k'} \quad (3)$$

whereas the attenuation α was given by the slope of the linear regression applied on the natural logarithm of the absolute $U_y(x)$ waveform (Catheline et al., 2004)

$$\alpha=\underset{\alpha}{\operatorname{argmin}}\left\|\ln[abs(U_y)]-(\alpha x+b)\right\|_2^2. \quad (4)$$

Without any assumption on the viscoelastic behavior of experimental data, the complex shear modulus $G(\omega)$ and wave number $k=k'+i\alpha$ are related through the shear wave propagation equation as

$$G(\omega)=\rho\frac{(2\pi\times f_{wave})^2}{k^2} \quad (5)$$

where f_{wave} is the frequency of the harmonic shear wave. As shown (Vappou et al., 2009), the real and imaginary parts of Eq. (5) can be rewritten as

$$G'(\omega)=\rho\omega^2\frac{k'^2-\alpha^2}{(k'^2+\alpha^2)^2} \quad (6)$$

$$G''(\omega)=-2\rho\omega^2\frac{k'\alpha}{(k'^2+\alpha^2)^2} \quad (7)$$

Using Eqs. (6) and (7), the storage $G'(\omega)$ (elastic behavior) and loss $G''(\omega)$ (viscous behavior) moduli were calculated from the wave velocity and attenuation (Eqs. (3) and (4)).

2.4. Summary of data processing

As illustrated in Fig. 2, the first step consisted in computing spatio-temporal blood clot displacements induced by shear waves using a normalized cross-correlation (NCC) algorithm applied to the RF temporal sequence ($I_{RF}(x,y,t)$). For each pixel of the time-varying displacement waveform, a Fourier transform (FT) was computed and the corresponding complex spectral amplitude at the generated frequency was used to form the complex stationary displacement field. The wave number k' was retrieved at each depth y by applying a second spatial Fourier transform to the real part of the stationary displacement field at the corresponding depth, to obtain the wave velocity v in Eq. (3). On the other hand, the wave attenuation α at each depth was linearly interpolated according to Eq. (4) using the natural logarithm (ln) of the absolute part of the complex value of the stationary displacement field at the corresponding depth. Finally, with Eqs. (6) and (7), we deduced G' and G''.

2.5. Modeling of the viscoelasticity behavior

Model fittings of $G'(\omega)$ and $G''(\omega)$ were used to deduce elasticity (μ) and viscosity (η) moduli of blood clots. Equations and schematic representations of each viscoelastic model are presented in Fig. 3. Rheological laws varied according to their level of complexity, ranging from the simplest (Maxwell and Kelvin–Voigt) to higher-order models (Jeffrey and Zener). Moreover, a generalized model (third-order generalized Maxwell), considering series-parallel viscosities and elasticities, was also tested. These five models were fitted to the experimental data by minimizing the error χ as a function of viscoelastic parameters (μ_i, η_i)

$$\chi=\left\|G'(\omega)-\hat{G}'(\omega)\right\|_2+\left\|G''(\omega)-\hat{G}''(\omega)\right\|_2 \quad (8)$$

where $\hat{G}'(\omega)$ and $\hat{G}''(\omega)$ are fitted theoretical storage and loss moduli of each model (Fig. 3). In Eq. (8), the non-linear least square minimization of χ was done with the *Lsqnonlin* function of Matlab (The MathWorks Inc., Natick, MA, USA, version 6.5) for each frequency. After convergence of the solution, the resulting parameter χ^* denoted the best-fit between models and experimental data. Note that the optimization problem was built with the complex shear modulus instead of v and α because G' and G'', unlike wave velocity and attenuation, have the same unit and a similar range of values, which avoided numerical instability during the inverse problem-solving.

3. Results

Typical kinetics of blood viscoelasticity (G', G'') during coagulation are presented in Fig. 4 for 3 experiments with animal #1. Experimental means and standard deviations (STD) were calculated from measurements at 20 different depths (y direction, Fig. 1), between $y=27.5$ mm and $y=47.7$ mm. Because G' and G'' assessment presents significant variability for incipient clots (semi-liquid material), these parameters could only be estimated for time starting from 30 to 40 min after the addition of calcium. All plots can be typified by a strong increment in G' with maximum changes

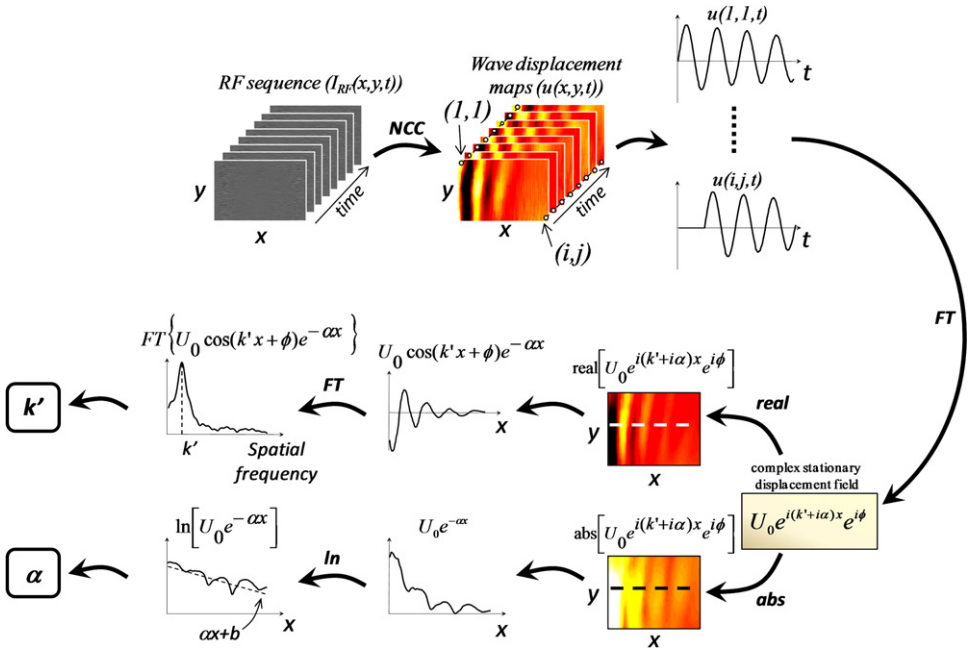

Fig. 2. Block-diagram of the data processing for the calculation of the wave number k' and the attenuation α from RF sequences (see text for details).

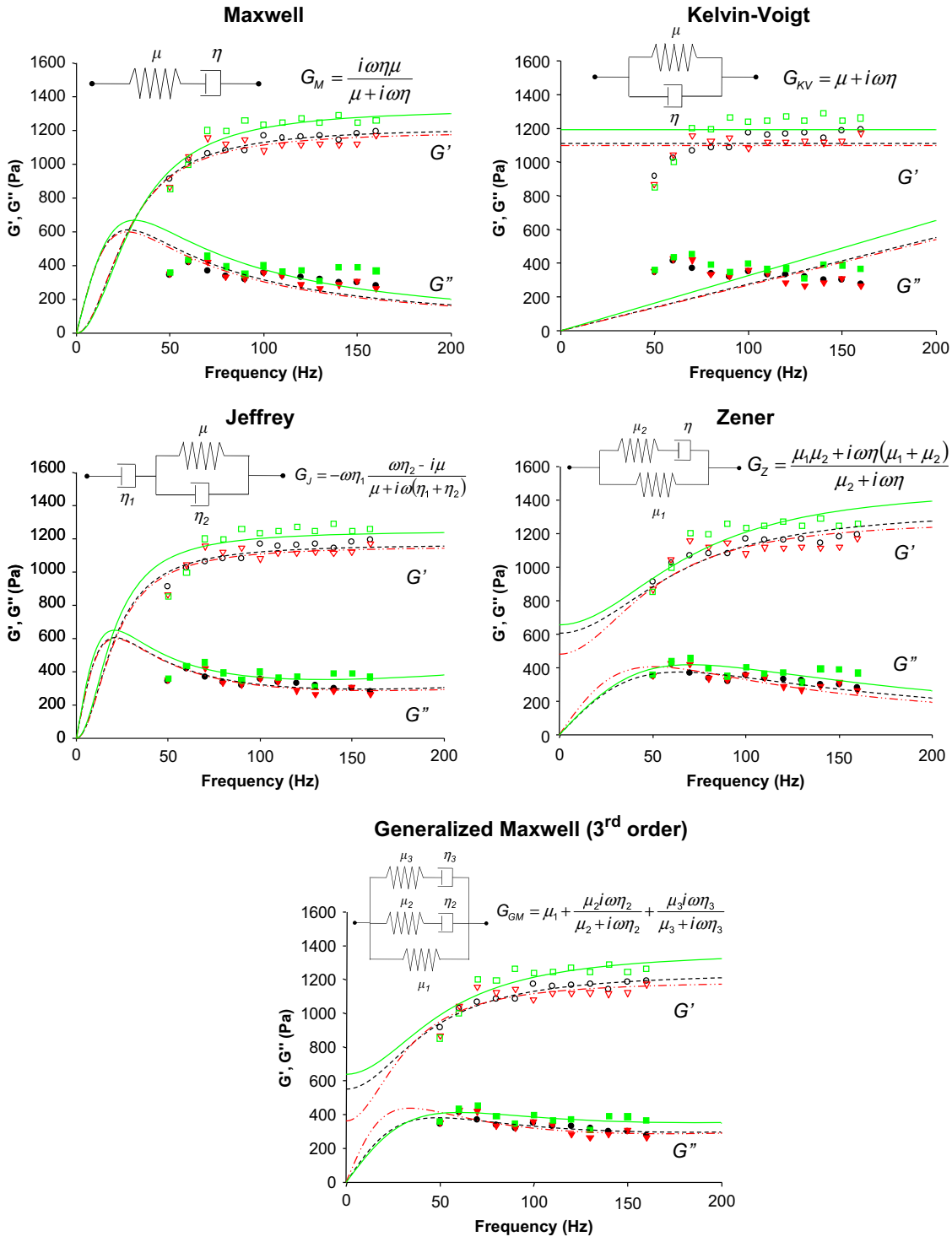

Fig. 3. Experimental (symbols) and simulated (line graphs) storage (G', open symbols) and loss (G'', filled symbols) modulus dispersions of blood clots (samples from animal #1). Simulated fittings correspond to Maxwell, Kelvin–Voigt, Jeffrey, Zener, and third-order generalized Maxwell models. Experiment 1 (data: black circles; fitting: black dashed line graphs), experiment 2 (data: red triangles-down; fitting: red dashed-dotted line graphs) and experiment 3 (data: green squares; fitting: green solid line graphs). (For interpretation of the references to color in this figure legend, the reader is referred to the web version of this article.)

in elasticity at the beginning of estimation ($G'\ slope^i_{max} = 27.0 \pm 10.4$ Pa/min), and quasi-stabilization after 120 min (G'^i_{max} between 1030 and 1240 Pa). G'' presented very different trends with quite constant evolution until a sudden maximum at t^i_e (between 38 and 81 min) followed by a decrease to $G''^i_{plateau}$. Results of G'_{max}, $G'\ slope_{max}$, t_e and $G''_{plateau}$ of all animal bloods served to calculate intra-animal (IntraAD, $n=3$) and inter-animal (InterAD, $n=3$) dispersions (Calle et al., 2009). As seen in Table 1, IntraAD and InterAD were, respectively, 9.1% and 15.9% for G'_{max}, 21.9% and 40.4% for $G'\ slope_{max}$, 18.7% and 27.4% for t_e, and largest dispersions were 40.2% and 58.6% for $G''_{plateau}$.

Examples of storage and loss moduli of formed clots (after 3 h) as a function of frequency are plotted in Fig. 3 for animal #1 (3 experiments) along with fitted rheological models for each of these experiments. G' and G'' varied with frequency, especially G' that presented a significant increase from 877 ± 31 Pa at 50 Hz to

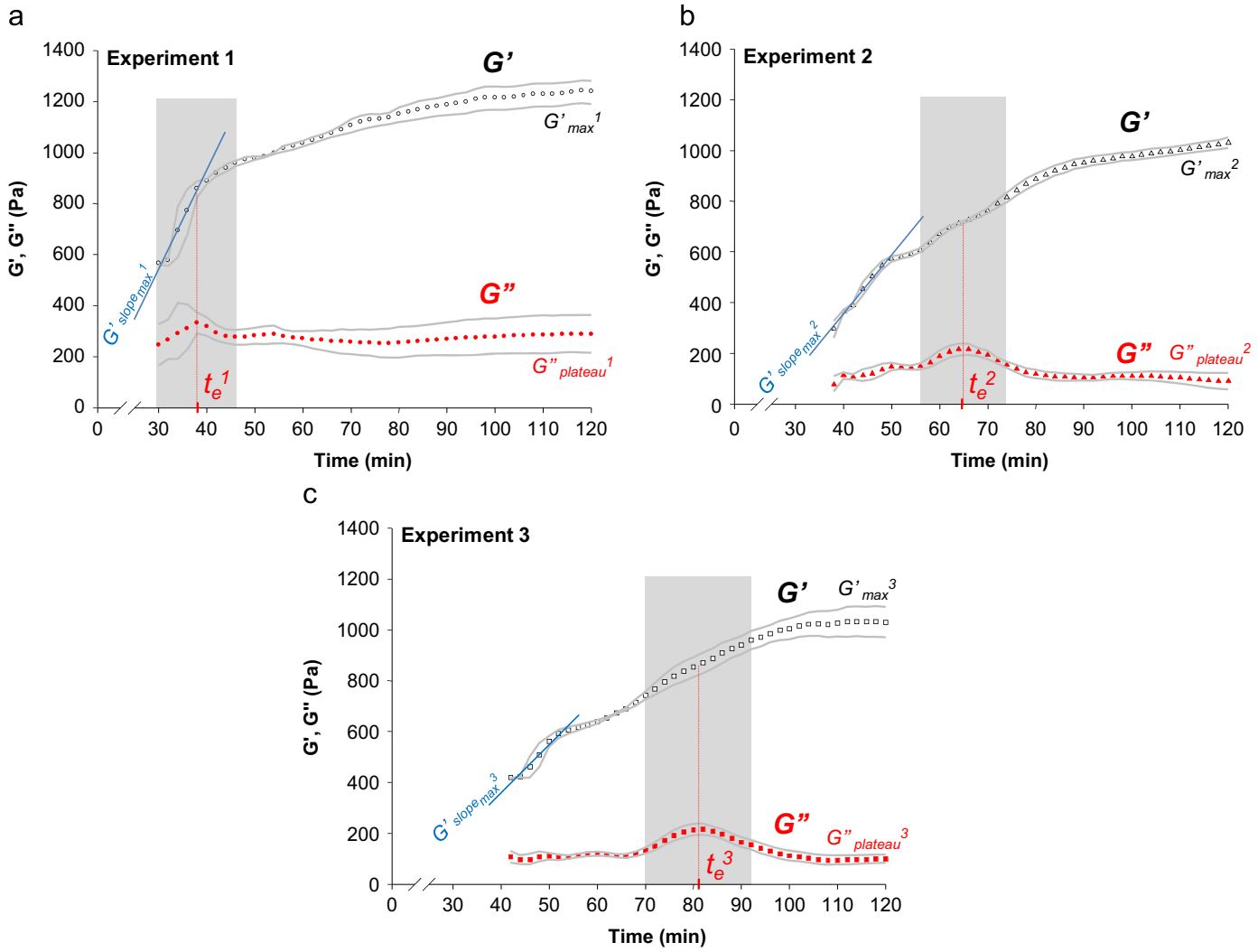

Fig. 4. . Time-varying storage G' (open symbols) and loss G'' (filled symbols) moduli of blood during clotting for 3 experiments (a, b, c) with blood samples withdrawn from the same pig (animal #1). Experimental means (symbols) and corresponding standard deviations (gray solid line graphs) were calculated from measurements at 20 different depths following the y-axis depicted in Fig. 1. G' $slope^{i}_{max}$ and G'^{i}_{max} describing G' evolution is displayed on each panel. $G''^{i}_{plateau}$ indicating the value of G'' at the plateau after 120 min of coagulation, the region of G'' inflexion (gray box), and the time t^{i}_{e} corresponding to the maximum of G'' are also plotted on each panel.

Table 1
Mean values and intra- and inter-animal dispersions of G'_{max}, G' $slope_{max}$, t_e and $G''_{plateau}$ rheological parameters.

	Mean	SD/mean (%)	
		Intra	Inter
G'_{max} (Pa)	953.9	± 9.1	± 15.9
G' $slope_{max}$ (Pa/min)	21.3	± 21.9	± 40.4
t_e (min)	69.6	± 18.7	± 27.4
$G''_{plateau}$ (Pa)	167.8	± 40.2	± 58.6

1208 ± 47 Pa at 160 Hz. Similar viscoelastic curves were obtained for all 9 experiments (3 animals) with corresponding averaged variability over frequency for G' and G'', defined as STD/mean, respectively, of 5.5 ± 1.7% and 9.5 ± 5.6% (animal #1), 6.8 ± 3.0% and 9.7 ± 7.3% (animal #2), and 9.2 ± 0.8% and 12.5 ± 12% (animal #3).

The best fitted viscoelastic parameters for all rheological models and corresponding residues χ^* (Eq. (8)) are reported in Table 2. Except for the Maxwell and Jeffrey equations, which could not fit G'' at 50 Hz, or the Kelvin–Voigt model which is not adapted to fit both G' and G'' curves (Fig. 3), other models could qualitatively describe blood clot viscoelasticity. Moreover, averaged intra-animal viscoelastic parameter (μ_i, η_i) dispersions were found to be 8.0 ± 2.4%, 7.8 ± 2.0%, 13.3 ± 6.2%, 13.2 ± 6.0%, and 27.0 ± 19.1% for Maxwell, Kelvin–Voigt, Jeffrey, Zener and generalized Maxwell models, whereas averaged inter-animal dispersions were 19.7 ± 5.9%, 24.7 ± 18.3%, 28.0 ± 20.5%, 51.6 ± 36.6% and 57.9 ± 27.0% for these same models. Regarding residues χ^* of Table 2, Maxwell (χ^* = 71.4 Pa) and Kelvin–Voigt (χ^* = 86.2 Pa) laws gave mean residues that were about twice values of other models (mean $\chi^* \leq$ 46.6 Pa).

An analysis of variance (one-way ANOVA with the Bonferroni post hoc test) applied on residues (Fig. 5) revealed a significant difference ($p < 0.05$) between the group composed of the Maxwell and Kelvin–Voigt models and the generalized Maxwell model, while such a significant difference ($p < 0.05$) could also be observed between the Kelvin–Voigt and higher-order explored viscoelastic laws (Jeffrey, Zener and generalized Maxwell).

4. Discussion and conclusion

This study aimed demonstrating *in vitro* that the generation and tracking of harmonic plane shear waves into a blood clot can characterize its kinetics of coagulation and rheological behavior. To

Table 2
Blood clot frequency dependence model fitting with mean elasticity and viscosity parameters and corresponding standard deviations (in parenthesis) for 3 experiments in 3 animals. Residue χ^* for the best-fitting mechanical parameters is also given.

Viscoelastic models		Animal 1 ($n=3$)	Animal 2 ($n=3$)	Animal 3 ($n=3$)	Mean
Maxwell	μ (Pa)	1250.78 (70.50)	958.16 (89.28)	973.16 (41.86)	1060.70 (164.78)
	η (Pa.s)	6.95 (0.09)	11.11 (0.93)	8.44 (1.55)	8.83 (2.10)
	χ^* (Pa)	78.68 (13.06)	54.12 (4.07)	81.26 (18.02)	71.35 (14.98)
Kelvin–Voigt	μ (Pa)	1134.13 (50.60)	933.74 (85.91)	928.67 (52.68)	998.84 (117.18)
	η (Pa.s)	0.47 (0.05)	0.22 (0.02)	0.31 (0.03)	0.33 (0.12)
	χ^* (Pa)	144.26 (12.10)	46.93 (8.16)	67.46 (8.80)	86.22 (51.30)
Jeffrey	μ (Pa)	1235.16 (58.37)	947.21 (90.74)	955.79 (48.71)	1046.05 (163.82)
	η_1 (Pa.s)	9.51 (0.64)	30.11 (6.27)	20.16 (4.01)	19.92 (10.30)
	η_2 (Pa.s)	0.17 (0.04)	0.15 (0.01)	0.21 (0.03)	0.17 (0.03)
	χ^* (Pa)	53.93 (16.65)	32.00 (1.29)	46.60 (18.34)	44.18 (11.16)
Zener	μ_1 (Pa)	578.20 (90.59)	805.20 (44.11)	771.79 (48.19)	718.39 (122.55)
	μ_2 (Pa)	796.36 (46.12)	319.06 (20.43)	449.99 (57.78)	521.80 (246.62)
	η (Pa.s)	2.07 (0.39)	0.44 (0.14)	0.54 (0.08)	1.01 (0.91)
	χ^* (Pa)	63.18 (14.07)	22.17 (1.17)	54.47 (14.87)	46.61 (21.61)
Generalized Maxwell	μ_1 (Pa)	518.42 (140.82)	797.76 (40.70)	629.15 (145.16)	648.44 (43.06)
	μ_2 (Pa)	1.30×10^{15} (0.34×10^{15})	8.49×10^{14} (3.66×10^{14})	969.88 (409.16)	7.16×10^{14} (12.32×10^{8})
	η_2 (Pa.s)	0.13 (0.01)	0.08 (0.01)	0.20 (0.02)	0.14 (0.04)
	μ_3 (Pa)	748.66 (71.40)	216.79 (39.65)	316.13 (126.59)	427.19 (302.15)
	η_3 (Pa.s)	2.95 (1.03)	0.51 (0.25)	2.00 (1.85)	1.82 (1.9)
	χ^* (Pa)	45.25 (16.65)	15.51 (2.21)	40.71 (20.48)	33.82 (16.02)

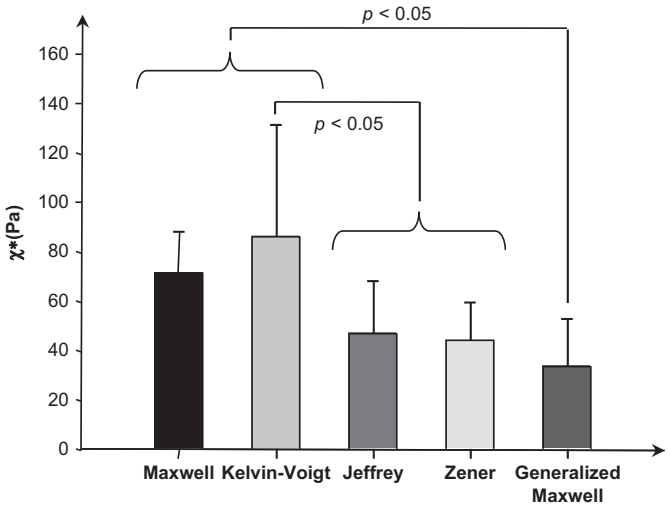

Fig. 5. . Model fitting residues χ^* for Maxwell, Kelvin–Voigt, Jeffrey, Zener and generalized Maxwell rheological laws (results for all animal data, $n=9$).

our knowledge, this is the first work dedicated to quantitatively assess G' and G'' of fresh whole blood, both during the clotting process and after complete coagulation at such frequency ranges (70 Hz during coagulation and between 50 and 160 Hz after 3 h of clotting).

4.1. Viscoelasticity evolution during blood coagulation

Both storage and loss moduli were sensitive to clot formation, but could not be measured at the early stage ($<$30–40 min after the coagulation cascade initiation). Indeed, in the presence of incipient blood clots, measurement accuracy was strongly affected by 2 mechanical considerations: the strong wave attenuation (low signal-to-noise ratio) due to significant blood clot viscosity, and the difficulty in measuring very short wavelengths in very soft immature clots filling only a limited volume of the phantom inclusion.

As clearly seen in Fig. 4 and also for experiments with blood animals #2 and #3 (data not shown), G'' stabilized very quickly compared to G' curves. The G' evolution is comparable to results obtained with 1-D transient ultrasound elastography (Gennisson et al., 2006a) and in rheometry (Tynngard et al., 2006; Williams et al., 2006; Evans et al., 2008b). As noted in Table 1, the temporal evolution of elasticity reached a mean value of 953.9 Pa (after 120 min of coagulation). Since no previous works had similar conditions (animal vs. human blood, blood sample volume, frequency range, hematocrit, etc.), quantitative comparison with the literature is difficult.

Interestingly, the difference in gelation stabilization time between G' and G'' reported in Fig. 4 is supported by a model describing the kinetics of blood clot structure formation (Kaibara, 1996). As proposed in that model, the increase in G'' is attributed to the conversion of the fibrin monomer to fibrin polymer, followed by an increment in G' because of fibrin network formation from fibrin polymer. During coagulation, we also observed a transient increase in G'' that could be accompanied by an inflection in the G' rate of increase (gray zones in Fig. 4). This phenomenon may be due to clot retraction. Indeed, around 30–60 min after blood clots begin to form, platelets entrapped within the fibrin network shrink because of protein activity and contractile force (Carr, Jr., 2003). As a result, the clot diminishes in size, expelling free serum (seen experimentally during blood coagulation). A similar clot retraction phase was also detected in mechanical rheometry measurements of shear moduli (Williams et al., 2006; Evans et al., 2008b), or by acoustic methods quantifying sound velocity (Libgot-Calle et al., 2008) or integrated attenuation coefficient (Calle et al., 2009). These latter acoustic studies confirmed that this sudden, small "thrust" occurred at the precise moment of serum expulsion. Note that the time apparition of such G'' modal increase at t_e could be affected by the initial blood composition, by the age of the sample (Solheim et al., 2004; Uyuklu et al., 2009) or by chemical interactions between the agar-gelatin block surface of the phantom and the blood sample.

4.2. Blood clot rheological behavior

Among five rheological models that differ from each other by their level of complexity (2 to 5 viscoelastic parameters), residue calculation proved statistically ($p<0.05$, Fig. 5) that the Kelvin–Voigt model

is less adapted to characterize blood clot dynamic behaviors. This allows to conclude that such a simple 2-parameter model, contrary to the simplifying assumption made by us and others (Viola et al., 2004; Gennisson et al., 2006a), cannot predict the viscoelasticity of whole porcine blood clots in the frequency range of 50–160 Hz.

As listed in Table 2, the residue χ^* averaged over all measurements (9 experiments) was minimum for the generalized Maxwell model. However, the second elastic modulus (μ_2) of that model tended to infinity for animals #1 and #2. This implies convergence of the generalized Maxwell law towards a 4-parameter viscoelastic model equivalent to Kelvin–Voigt in parallel with Maxwell. Moreover, the fit of G' and G'' by such 4-parameter model (3 elasticities and 1 viscosity) did not improve results compared to the generalized Maxwell model, since the calculated residue χ^* of 34.05 ± 19.04 Pa was superior to χ^*_{GM}. Third-order models of this study (Jeffrey and Zener) may thus be considered advantageous because stable (realistic finite estimates) second-order elasticity or viscosity parameters allowed independently to adjust storage and loss moduli to consider strong stiffness dispersion over frequency, significant viscosity at low frequencies, or local frequency profile irregularities. However, recent studies with human whole blood reported interesting results that typified clot viscoelasticity evolution over excitation frequencies ranging from 0.1 to 10 Hz (Williams et al., 2006; Evans et al., 2008b). Elastic and viscous parameters increasing with frequency were shown. At quasi-static frequency (0.1 Hz), G' was different from zero, suggesting that only Zener and generalized Maxwell models could be valid (see Fig. 3 for extrapolation at a frequency of zero). According to the above-mentioned discussion, the Zener model is thus recommended to typify blood clot viscoelasticity.

Other experiments (Roberts et al., 1974), with platelet-rich plasma, concluded that the elasticity remains nearly constant over the 0.01 to 160 Hz frequency range, whereas the loss modulus is proportional to frequency. These results, compared to ours, highlight the impact of red blood cells on clot mechanical properties. Indeed, viscoelastic characterization of individual human erythrocytes in the 0.1 to 100 Hz frequency range, by magnetic twisting cytometry, disclosed a nearly frequency-independent apparent storage modulus up to 30 Hz, while the loss modulus increased as a power law (Puig-de-Morales-Marinkovic et al., 2007). Because blood clot samples characterized in our study comprise trillions of red blood cells entrapped in a dense fibrin network, it is very complex to draw a parallel with independent dynamic mechanical behavior of individual red blood cells. Most importantly, the data reported here also permitted to explore the effect of red blood cells on the dynamic mechanical behavior of blood clots, which could be the key of novel medication strategy for DVT management.

Conflict of interest statement

None of the authors in this work has conflict of interests with other people and organizations.

Acknowledgements

This research was supported by a grant from the Canadian Institutes of Health Research (#MOP-84358). Cédric Schmitt received a partial Ph.D. scholarship and Dr. Anis Hadj Henni, a partial post-doctoral fellowship, from the Groupe de recherche en sciences et technologies biomédicales of the Institute of Biomedical Engineering of the University of Montreal. The authors thank J. Brochu from "Les Viandes ULTRA Meats Inc." for blood supplies. The editorial assistance of Dr. Ovid Da Silva, Research Support Office, CHUM Research Centre, is acknowledged.

References

Achenbach, J.D., 1973. Wave propagation in elastic solids. North-Holland, Amsterdam, pp. 100–145.
Bercoff, J., Tanter, M., Fink, M., 2004. Supersonic shear imaging: a new technique for soft tissue elasticity mapping. IEEE Trans. Ultrason. Ferroelectr. Freq. Control 51 (4), 396–409.
Bossy, E., Funke, A.R., Daoudi, K., Boccara, A.C., Tanter, M., Fink, M., 2007. Transient optoelastography in optically diffusive media. Appl. Phys. Lett. 90 (17), 174111.
Bouchard, R.R., Palmeri, M.L., Pinton, G.F., Trahey, G.E., Streeter, J.E., Dayton, P.A., 2009. Optical tracking of acoustic radiation force impulse-induced dynamics in a tissue-mimicking phantom. J. Acoust. Soc. Am. 126 (5), 2733–2745.
Burghardt, W.R., Goldstick, T.K., Leneschmidt, J., Kempka, K., 1995. Nonlinear viscoelasticity and the thrombelastograph: 1. Studies on bovine plasma clots. Biorheology 32 (6), 621–630.
Calle, R., Plag, C., Patat, F., Ossant, F., 2009. Interest of the attenuation coefficient in multiparametric high frequency ultrasound investigation of whole blood coagulation process. J Acoust. Soc. Am. 125 (1), 530–538.
Carr Jr., M.E., 2003. Development of platelet contractile force as a research and clinical measure of platelet function. Cell Biochem. Biophys. 38 (1), 55–78.
Catheline, S., Gennisson, J.L., Delon, G., Fink, M., Sinkus, R., Abouelkaram, S., Culioli, J., 2004. Measuring of viscoelastic properties of homogeneous soft solid using transient elastography: an inverse problem approach. J Acoust. Soc. Am. 116 (6), 3734–3741.
Evans, P.A., Hawkins, K., Lawrence, M., Williams, R.L., Barrow, M.S., Thirumalai, N., Williams, P.R., 2008a. Rheometry and associated techniques for blood coagulation studies. Med. Eng. Phys. 30 (6), 671–679.
Evans, P.A., Hawkins, K., Williams, P.R., Williams, R.L., 2008b. Rheometrical detection of incipient blood clot formation. J. Non-Newtonian Fluid Mech. 148, 122–126.
Geier, B., Barbera, L., Muth-Werthmann, D., Siebers, S., Ermert, H., Philippou, S., Mumme, A., 2005. Ultrasound elastography for the age determination of venous thrombi. Evaluation in an animal model of venous thrombosis. Thromb. Haemost. 93 (2), 368–374.
Gennisson, J.L., Lerouge, S., Cloutier, G., 2006a. Assessment by transient elastography of the viscoelastic properties of blood during clotting. Ultrasound Med Biol. 32 (10), 1529–1537.
Gennisson, J.L., Cloutier, G., 2006b. Sol–gel transition in agar-gelatin mixtures studied with transient elastography. IEEE Trans. Ultrason. Ferroelectr. Freq. Control 53 (4), 716–723.
Hadj Henni, A., Schmitt, C., Cloutier, G., 2008. Three-dimensional transient and harmonic shear-wave scattering by a soft cylinder for dynamic vascular elastography. J. Acoust. Soc. Am. 124 (4), 2394–2405.
Kaibara, M., 1996. Rheology of blood coagulation. Biorheology 33 (2), 101–117.
Kruse, S.A., Smith, J.A., Lawrence, A.J., Dresner, M.A., Manduca, A., Greenleaf, J.F., Ehman, R.L., 2000. Tissue characterization using magnetic resonance elastography: preliminary results. Phys. Med. Biol. 45 (6), 1579–1590.
Libgot-Calle, R., Ossant, F., Gruel, Y., Lermusiaux, P., Patat, F., 2008. High frequency ultrasound device to investigate the acoustic properties of whole blood during coagulation. Ultrasound Med. Biol. 34 (2), 252–264.
Muthupillai, R., Lomas, D.J., Rossman, P.J., Greenleaf, J.F., Manduca, A., Ehman, R.L., 1995. Magnetic-resonance elastography by direct visualization of propagating acoustic strain waves. Science 269 (5232), 1854–1857.
Nahirnyak, V.M., Yoon, S.W., Holland, C.K., 2006. Acousto-mechanical and thermal properties of clotted blood. J. Acoust. Soc. Am. 119 (6), 3766–3772.
Puig-de-Morales-Marinkovic, M., Turner, K.T., Butler, J.P., Fredberg, J.J., Suresh, S., 2007. Viscoelasticity of the human red blood cell. Am. J. Physiol. Cell Physiol. 293 (2), C597–C605.
Riha, P., Wang, X., Liao, R., Stoltz, J.F., 1999. Elasticity and fracture strain of whole blood clots. Clin. Hemorheol. Microcirc. 21 (1), 45–49.
Roberts, W.W., Kramer, O., Rosser, R.W., Nestler, F.H.M., Ferry, J.D., 1974. Rheology of fibrin clots. I. Dynamic viscoelastic properties and fluid permeation. Biophys. Chem. 1 (3), 152–160.
Sandrin, L., Tanter, M., Catheline, S., Fink, M., 2002. Shear modulus imaging with 2-D transient elastography. IEEE Trans. Ultrason. Ferroelectr. Freq. Control 49 (4), 426–435.
Sarvazyan, A.P., Rudenko, O.V., Swanson, S.D., Fowlkes, J.B., Emelianov, S.Y., 1998. Shear wave elasticity imaging: a new ultrasonic technology of medical diagnostics. Ultrasound Med. Biol. 24 (9), 1419–1435.
Sinkus, R., Lorenzen, J., Schrader, D., Lorenzen, M., Dargatz, M., Holz, D., 2000. High-resolution tensor MR elastography for breast tumour detection. Phys. Med. Biol. 45 (6), 1649–1664.
Solheim, B.G., Flesland, O., Seghatchian, J., Brosstad, F., 2004. Clinical implications of red blood cell and platelet storage lesions: an overview. Transfus. Apher. Sci. 31 (3), 185–189.
Taylor, L.S., Porter, B.C., Rubens, D.J., Parker, K.J., 2000. Three-dimensional sonoelastography: principles and practices. Phys. Med. Biol. 45 (6), 1477–1494.
Tynngard, N., Lindahl, T., Ramstrom, S., Berlin, G., 2006. Effects of different blood components on clot retraction analysed by measuring elasticity with a free oscillating rheometer. Platelets 17 (8), 545–554.

Uyuklu, M., Cengiz, M., Ulker, P., Hever, T., Tripette, J., Connes, P., Nemeth, N., Meiselman, H.J., Baskurt, O.K., 2009. Effects of storage duration and temperature of human blood on red cell deformability and aggregation. Clin. Hemorheol. Microcirc. 41 (4), 269–278.

Vappou, J., Maleke, C., Konofagou, E.E., 2009. Quantitative viscoelastic parameters measured by harmonic motion imaging. Phys. Med. Biol. 54 (11), 3579–3594.

Viola, F., Kramer, M.D., Lawrence, M.B., Oberhauser, J.P., Walker, W.F., 2004. Sonorheometry: a noncontact method for the dynamic assessment of thrombosis. Ann. Biomed. Eng. 32 (5), 696–705.

Williams, P.R., Hawkins, K., Wright, C., Evans, A., Simpkin, H., Barrow, M.S., Williams, R.L., 2006. Rheometrical and computational studies of blood viscoelasticity during coagulation. Clin. Hemorheol. Microcirc. 35 (1-2), 123–127.

Xie, H., Kim, K., Aglyamov, S.R., Emelianov, S.Y., O'Donnell, M., Weitzel, W.F., Wrobleski, S.K., Myers, D.D., Wakefield, T.W., Rubin, J.M., 2005. Correspondence of ultrasound elasticity imaging to direct mechanical measurement in aging DVT in rats. Ultrasound Med. Biol. 31 (10), 1351–1359.

Zwiebel, W.J., 2004. "Ultrasound diagnosis of venous thrombosis,". In: Zwiebel, W.J., Pellerito, J.S. (Eds.), Introduction to Vascular Ultrasonography fifth ed.. Elsevier Science, pp. 449–465.